Lab on a Chip

PAPER

View Article Online
View Journal | View Issue

Cite this: *Lab Chip*, 2021, **21**, 4379

Interaction between positive and negative dielectric microparticles/microorganism in optoelectronic tweezers†

Shuzhang Liang, ‡[a] Chunyuan Gan,‡[a] Yuguo Dai,[a] Chaonan Zhang,[a] Xue Bai,[a] Shuailong Zhang, [bc] Aaron R. Wheeler, [def] Huawei Chen *[ag] and Lin Feng*[ag]

Optoelectronic tweezers (OET) is a noncontact micromanipulation technology for controlling microparticles and cells. In the OET, it is necessary to configure a medium with different electrical properties to manipulate different particles and to avoid the interaction between two particles. Here, a new method exploiting the interaction between different dielectric properties of micro-objects to achieve the trapping, transport, and release of particles in the OET system was proposed. Besides, the effect of interaction between the micro-objects with positive and negative dielectric properties was simulated by the arbitrary Lagrangian–Eulerian (ALE) method. In addition, compared with conventional OET systems relying on fabrication processes involving the assembly of photoelectric materials, a contactless OET platform with an iPad-based wireless-control interface was established to achieve convenient control. Finally, this platform was used in the interaction of swimming microorganisms (positive-dielectric properties) with microparticles (negative-dielectric properties) at different scales. It showed that one particle could interact with 5 particles simultaneously, indicating that the interaction can be applied to enhance the high-throughput transportation capacities of the OET system and assemble some special microstructures. Owing to the low power, microorganisms were free from adverse influence during the experiment. In the future, the interaction of particles in a simple OET platform is a promising alternative in micro–nano manipulation for controlling drug release from uncontaminated cells in targeted therapy research.

Received 11th July 2021,
Accepted 24th September 2021

DOI: 10.1039/d1lc00610j

rsc.li/loc

1. Introduction

Noncontact micromanipulation technology has been applied to various research fields, such as the analysis of biochemical processes and mechanistic studies.[1,2] In general, noncontact technologies involve the application of optical tweezers,[3] magnetic manipulation,[4–6] acoustic oscillation,[7] or dielectrophoresis (DEP) trapping.[8,9] Among them, optical tweezers have the advantage of nano-level manipulation accuracy[10] with 3D control and can be employed in various applications[11–13] due to the fact that they can trap microparticles with optical gradient forces under the dynamic control of an operating program. Therefore, the Nobel Prize in Physics 2018 was awarded to the inventors of optical tweezers. However, on account of high levels of optical power required by optical tweezers, intense Joule heating would be generated in their processor chips. Furthermore, their applicability is limited under such specific conditions as particle size. To overcome these limitations, optical tweezers and DEP technologies can be combined to obtain optoelectronic tweezing (OET), also known as optically induced dielectrophoresis, which is proposed by Chiou *et al.*[14] for the first time. On the ground that photons, rather than the direct photon-generated force, are employed in the OET to control the application of DEP force, a smaller power is required for the generation of trapping forces. Thus, it is extremely challenging to achieve 3D manipulation in the OET system. In addition, in OET systems, a fixed electrode configuration is employed to obtain excellent manipulation precision through the utilization of a projected micro-pattern

[a] *School of Mechanical Engineering & Automation, Beihang University, Beijing, 100191, China. E-mail: chenhw75@buaa.edu.cn, linfeng@buaa.edu.cn*
[b] *School of Mechatronical Engineering, Beijing Institute of Technology, Beijing, 100081, China*
[c] *Beijing Advanced Innovation Center for Intelligent Robots and Systems, Beijing Institute of Technology, Beijing, 100081, China*
[d] *Department of Chemistry, University of Toronto, 80 St George St., Toronto, ON, M5S 3H6, Canada*
[e] *Donnelly Centre for Cellular and Biomolecular Research, University of Toronto, 160 College St, Toronto, ON, M5S 3E1, Canada*
[f] *Institute for Biomaterials and Biomedical Engineering, University of Toronto, 164 College St, Toronto, ON, M5S 3G9, Canada*
[g] *Beijing Advanced Innovation Center for Biomedical Engineering, Beihang University, Beijing, 100191, China*

† Electronic supplementary information (ESI) available. See DOI: 10.1039/d1lc00610j

‡ These authors contributed equally to this work.

on the chip, which makes them outperform the flexibility of predesigned structures in conventional DEP systems. Since the development of OET, it has been applied in various engineering[15–18] and related applications.[19–23] For example, OET has been applied to fabricate applications with superior performance in the fields of energy storage and catalysis and sophisticated electronic devices, such as 3-D hydrogel microstructures containing different types of cells,[24] graphene macroassemblies,[25] and MoS_2 thin-film transistors.[26] Benefiting from OET, these devices could be fabricated by mask-free manners compared with photolithography and other traditional micro-nano fabricated techniques. Furthermore, an OET that contains a chip coated with the titanium oxide phthalocyanine (TiOPc) can be utilized to manipulate HepG2 cells,[21] while OETs using lithium niobate photoconductors have been used to create virtual electrodes through modulated illumination.[27] Meanwhile, it has been verified that an OET-based microrobot can be employed to select cells for RNA sequencing and other biomedical applications.[22] The OET is also adopted to analyze the relative hardness of red blood cells[28] and conditions that affect the cell membranes of swimming *Enterobacter aerogenes*.[29] The above-mentioned applications contribute to broadening the manipulation functions in the OET.

Although OET is a well-developed technology with excellent precision and versatility for micromanipulation purposes, there are certain potential shortcomings that would limit its application in some scenarios. For instance, in order to manipulate different micro-objects such as cells and microorganisms, the different dielectric property of the medium is required to configure. In addition, OET systems are prone to the effects of electrokinetic mechanisms, in which dielectric objects are polarized so that they are subjected to either positive or negative DEP.[30] While most microorganisms and cells are subject to positive DEP, and such objects as polystyrene microbeads are subject to negative DEP. Table 1 presents the DEP-related polarities in a medium of some micro-objects. Thus, the interaction of particles may occur when two particles approach each other[31] due to the laminar flow or non-flow of the medium in the OET chip. When many particles may adhere to each other, it would exert adverse impacts on the manipulation of particles or cells in the OET. Although there are some studies about the interactions between particles with DEP,[32–35] the interacted mechanism is not clearly explained. Especially, there is no theory currently to explain the interaction phenomenon in the OET system. Recently, Ai *et al.* have simulated the particle-particle interaction with the arbitrary Lagrangian–Eulerian method under DEP,[36] which is a more accurate analysis of the electrophoretic forces. Hwang *et al.* have found the electrostatic interactions between two particles in the OET.[31] However, the interactions in the OET are not fully explained by the simplified point dipole method, and the microstructure deformation in an electric field is also underestimated. For that reason, it is necessary to analyze and control the interactions between particles in the OET system and to reduce the trouble with medium configuration.

In this paper, a novel control approach was proposed in this research *via* exploiting the interaction between different dielectric properties of particles, in an attempt to achieve the trapping, transport, and release of micro-objects in the OET system, as shown in Fig. 1a and b. The simulation was performed on the effect of different dielectric properties of particles in the electric field and the interaction between particles by the ALE method, as shown in Fig. 1c and d. These key factors affecting the interaction were analyzed. In addition, a simple wireless OET platform was proposed with the capability to manipulate swimming microorganisms and micro-objects with differing dielectric properties at different scales. The platform was wirelessly controlled and configured in real-time with cloud data through an iPad interaction interface, as shown in Fig. 1a. With the adoption of the OET, positive-dielectric particles and microorganisms could interact with the negative-DEP microparticles by the light image in a microfluidic chip, as shown in Fig. 1b. Furthermore, the interaction of micro-objects was transported together to the target position. Through this approach, some problems involving the special treatment of microparticles were eliminated and the experimental contamination was decreased. It is expected to be used for drug release in targeted therapy research.

2. Results and discussions

2.1 Simulation of electric effects with single particle in OET

In the OET microfluidic chip, the light pattern induces the generation of a non-uniform electric field. When a dielectric particle is placed in a non-uniform electric field, the particle is polarized and subjected to DEP forces,[37] as shown in

Table 1 Polarities of particles subjected to dielectrophoretic force in OET medium

Types of micro-objects	Medium in microfluidic chip	Polarity of dielectrophoresis force
Polystyrene microspheres	Deionized water	Negative
Microrobot with Su-8 photoresist	Deionized water	Negative
Hydrogel	Deionized water	Negative
Erythrocyte	Cell culture medium	Positive
Cell	Cell culture medium	Negative
E. aerogenes	Dilute PBS	Positive
Euglena gracilis and spirulina	Deionized water	Positive

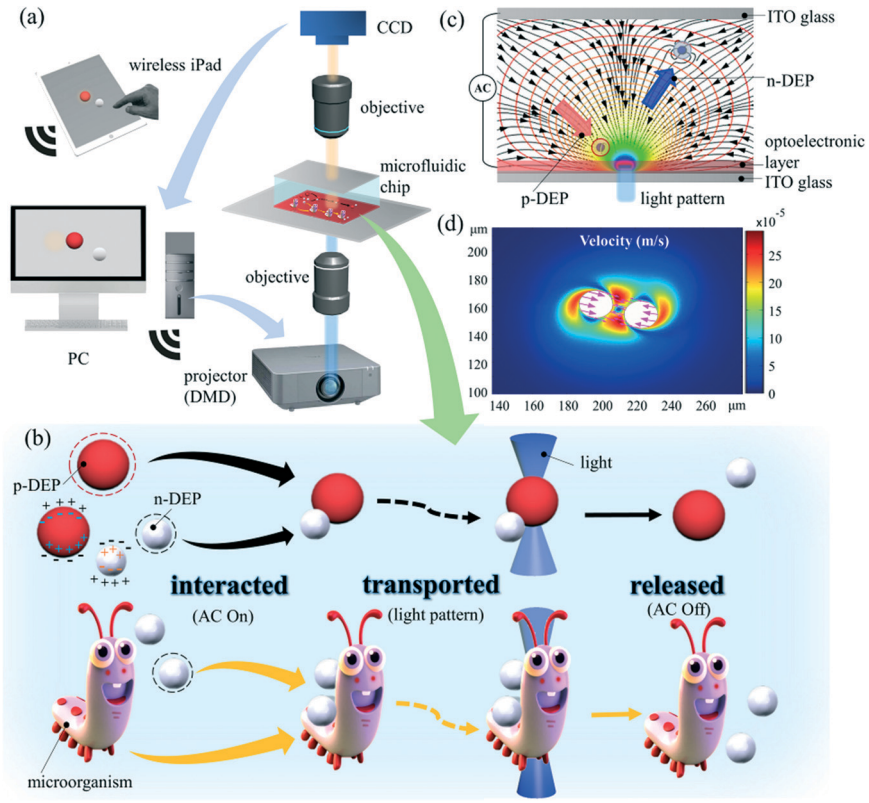

Fig. 1 Conceptual overview of controllable interaction between micro-objects and application for transportation of microparticles *via* OET. (a) A wireless OET manipulated platform with an iPad-based wireless-control. (b) Black arrow path: manipulation of positive-dielectric micro-object to adhere it to negative-dielectric microbead, which is then moved to transport the micro-object and microbead together. Yellow arrow path: manipulation of microorganism to adhere it to negative-dielectric microbead, which is then moved to transport the microorganism and microbead together by light pattern. (c) The different micro-objects suffer a different manipulated effect (positive DEP or negative DEP) in an OET. (d) Simulation of the interaction between micro-objects.

Fig. 2a. The inside electric field generated by the polarizing particles can be equivalent to a dipole moment composed of two source charges ($+q$ and $-q$). The dipole moment[38,39] is expressed as $p = 4\pi\varepsilon R^3 E$ (detail see the ESI† S1). Subsequently, the particles will move in the medium. There will be an interaction between the particle and flow field,[40] such as Stokes's drag force. Here, a finite-element software COMSOL 5.5 was introduced to simulate the coupled solid–fluid–electric field. The ALE method[41] was adopted to analyze particle characteristics in the coupled field. A light-induced dielectrophoresis model was applied to obtain the distribution of the electric field, as shown in Fig. 2b. The thickness of the medium space is 150 μm and the diameter of particle and light pattern is 20 μm, respectively. The input signal was a sine wave-shaped source (V_{pp} = 10 V, f = 2 kHz). The domain Ω is divided into a mesh of quadratic triangular elements. The particle surface and the channel wall have a higher density of mesh. The mesh can generate again in each step of the movement of the model to avoid the failure of the dividing of mesh. The numerical solutions would be converged when a relative error is smaller than 10^{-6} and the number of mesh is more than 25 000 in each model.

Fig. 2c and d show the electric properties of different particles and the distribution of electric fields in the medium when a light pattern is projected on the OET chip (particle 1: ε_1 = 2.56, σ_1 = 0.2 s m^{-1}; particle 2: ε_2 = 2.6, σ_2 = 2 × 10^{-4} s m^{-1}; medium: ε_m = 80, σ_m = 2 × 10^{-2} s m^{-1}). A strong electric field region is induced in the center of the light electrode. Then, the distribution of electric charges and electric polarization vector (black arrows) in the particle are used to analyze the different dielectric particle properties. These positive and negative electric charges are assembled on the opposite surface of the particle, respectively. The particle part near the light pattern is exposed to a higher polarization charge density than the farther part. It shows that a non-uniform electric field induces a nonhomogeneous polarization, equal to multipolar moment inside of particle.[42] Thus, the particle will be repelled from the light pattern in the n-DEP effect (blue arrows), and it will be attracted to the light pattern in the p-DEP effect (see Movie S1†). Particles are subjected to different DEP forces in this process. A light pattern can be employed to manipulate these particles. The particle pushed by the light spot in OET was also simulated, as shown in Fig. 2e, (see Movie S2†). The light pushes the particle from the left to right of the chip in the x-direction (black arrow). The building OET platform was applied to manipulate microparticles, as shown in Fig. 2f. As shown in this figure, magnetic microspheres with diameters of 20 μm

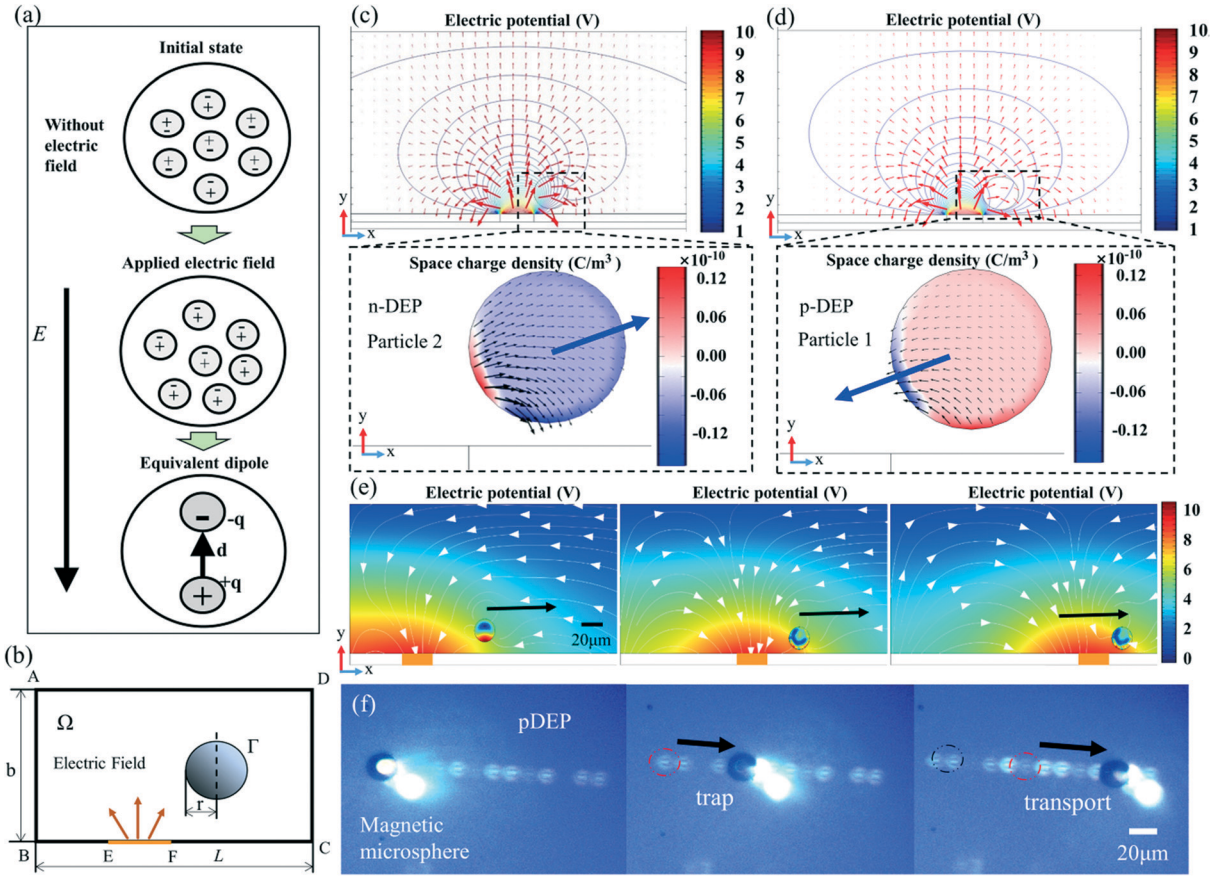

Fig. 2 The simulation of the electrical properties of particles with different properties in an electric field. (a) A dipole model of polarization particle. (b) A 2D schematic view of a particle in a chamber. An external electric field is applied between ITO glass BC and AD. (c) The electric potential and generated space charge density of particles with the negative property (particle 1: $\varepsilon_1 = 2.56$, $\sigma_1 = 0.2$ s m^{-1}. Particle 2: $\varepsilon_2 = 2.6$, $\sigma_2 = 2 \times 10^{-4}$ s m^{-1}. Medium: $\varepsilon_m = 80$, $\sigma_1 = 2 \times 10^{-2}$ s m^{-1}). (d) The electric potential and generated space charge density of particles with the positive property. (e) The simulation of the movement of particles experienced n-DEP force based on the ALE method. The surface inside the medium is electric potential (V). The surface of the particle is stress (N m^{-2}). (f) Transported particles experienced p-DEP force in OET.

are trapped by the light spot to move by a $10V_{pp}$ bias voltage with an AC frequency of 100 kHz. It can be demonstrated that the simulation results are consistent with the experimental results. For these different dielectric particles, the OET could achieve a different manipulated application, such as the sorting of particles.[43]

2.2 Simulation of the interaction between particles

In the OET system, when two polarized particles approach each other, they will interact with each other.[44] Based on that, an exploration was performed on an electric field simulation of the interaction between two particles with different dielectric properties (particle 1 and particle 2) and the same dielectric properties (particle 2 and particle 2). Fig. 3 presents the effect of different parameters on the interaction of two particles prior to contact. The schematic diagram of the interaction of both particles is shown in Fig. 3a. l represents the distance between the centers of the two particles. d represents the diameter of the particle. θ represents the angle that one particle rotates around another from a horizontal position. As shown in Fig. 3b, the dipole moment image model is used to analyze the interaction effect between two particles. Net dipole moment is expressed as $p_e = -\sum_{n=1}^{\infty} 2\left(q_n d_n + q'_n d'_n + q_c \lambda_n \xi_n\right)$. The mutual force is express as $F_m = (p_e \cdot \nabla)E$ (detail see the ESI† S1).

For the interaction effect, the position of the two particles plays a key factor. The conventional dipole moment model does not clearly present the dipole moment changing in the interaction process. An exploration was performed on the effects of the distance between two particles on the interaction dielectrophoresis force, as shown in Fig. 3e. In this simulation, the voltage was set as $10V_{pp}$ and the input frequency was set as 2 kHz, respectively. According to Newton's third law, the interacted forces between both particles are equal in magnitude and opposite in direction. DEP force of particle 1 was measured. The interaction between particles will be weakened with the increased distance between particles. When the particles are extremely close, the interaction force is of the same magnitude as the external electric field force. When the distance is beyond a

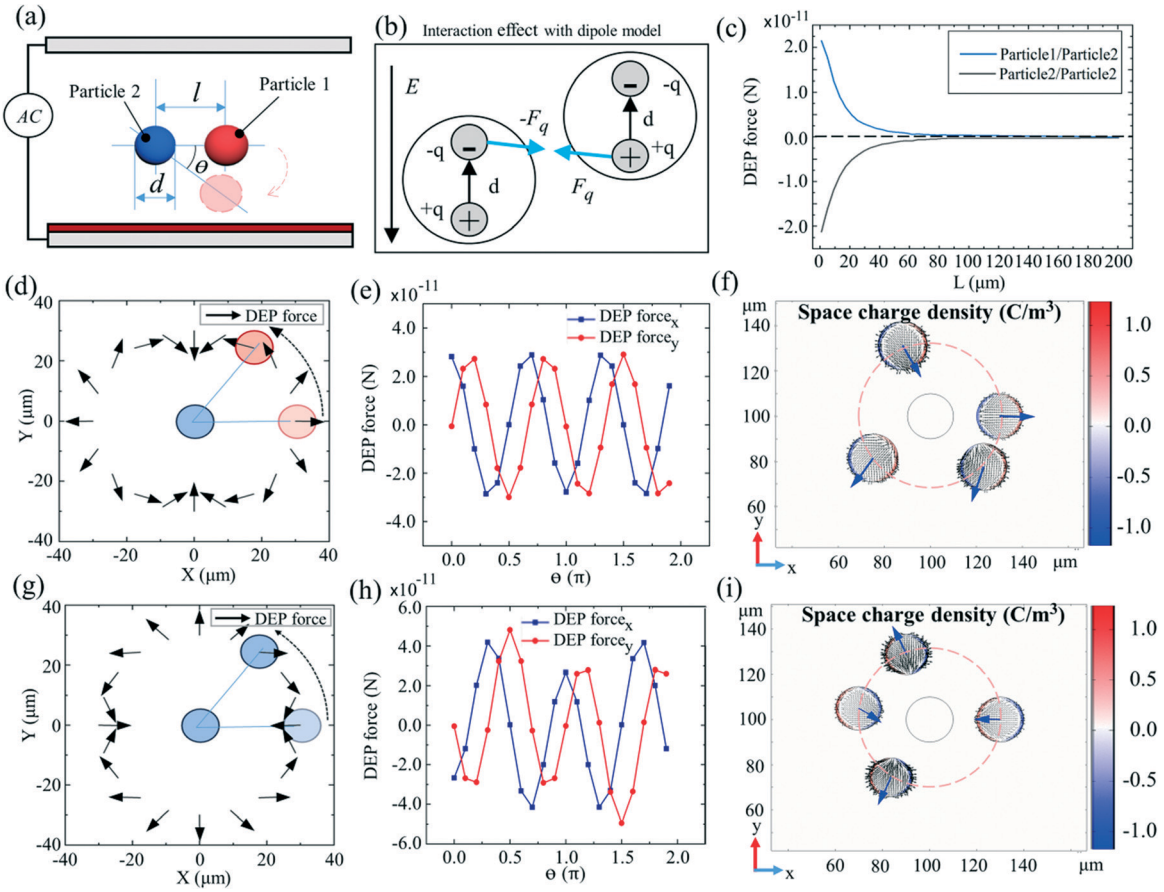

Fig. 3 Effects of the interaction between two particles in different positions. (a) Schematic diagram of the interaction between two particles. (b) A dipole interaction model between two particles. (c) The relationship between DEP force and distance of two particles. (d) The direction of an electric field force of interaction between positive and negative particles at different positions. (e) The x and y components force of interaction force between positive and negative particles at different positions. (f) The distribution of space charge density of the two microparticles when the positive particle interacts with the negative particle in different positions. (g) The direction of an electric field force of interaction between negative and negative particles at different positions. (h) The x and y components force of interaction force between negative and negative particles at different positions. (i) The distribution of space charge density of the two microparticles when the negative particle interacts with the negative particle at different positions.

threshold, the interaction effect could be ignored. In addition, due to the random position of particles in the medium, a simulation was performed on the direction of an electric field force of the interaction between particles at different positions, as shown in Fig. 3d–i. The distance between both particles was set as 30 μm. The results show that the magnitude of the force is constant and the direction is changing at every position. Therefore, the forces are characterized by the scattering in *X*- and *Y*-axes, as shown in Fig. 3e and h. The changes of force direction are periodical. When particle 1 has made one rotation around particle 2, the change period of the force direction is 3. At the opposite position of the rotated orbit, the direction of force is opposite. The direction of the interaction force between particle 1 and particle 2 is opposite to that between particle 2 and particle 2 at every position, which can also be demonstrated by the space charge distribution and polarization vector ***P*** (blue arrow), as shown in Fig. 3f and i. It shows that the polarization of particle 1 and particle 2 is opposite at the same moment of a period. The rotation can be seen in Movie S3.†

The simulated process of interaction and contact between two particles is also shown in Fig. 4a and b, (see Movie S4†). The pink arrow represents the velocity of particles in the interaction process. When the particles are attracted close to each other, the velocity will increase with the increase of the interaction force. Space charge distribution illustrates the attracted phenomenon in the process of interaction. The polarization direction of both particles is always pointing towards each other. The interaction of these two polystyrene microbeads is shown in Fig. 4c. Particles also generate a rotation under the torque effect in the OET.

2.3 Interaction between particle and particle

To improve the ability of the platform to precisely manipulate micro-objects so that they can control the interaction with each other, different approaches were applied to manipulate

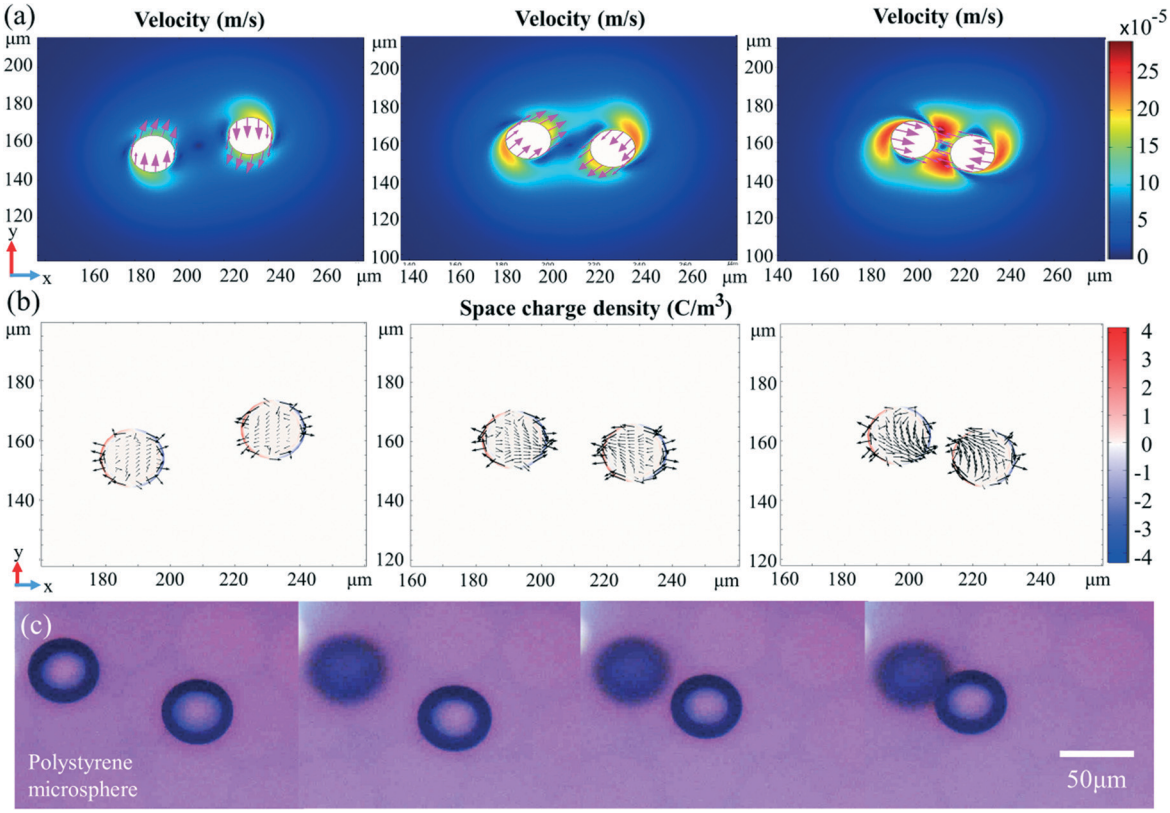

Fig. 4 The interaction between two microparticles. (a) The velocity of the two microparticles in the interaction process. The purple arrow represents the velocity vector. (b) The distribution of space charge density of the two microparticles in the interaction process. (c) The interaction of the two microparticles in the OET system.

microparticles with different dielectric properties. A schematic of interaction between positive microparticles (red sphere) and negative microparticles (blue sphere) is shown in Fig. 5a. The negative microparticles are fixed and the positive microparticles are manipulated to interact with them. In our previous manipulation experiment in the OET,[43] the magnetic microbeads are subjected to a p-DEP force (attracted to the light pattern), while the polystyrene microspheres are subjected to a n-DEP force (repelled by the light pattern). These two kinds of particles can interact with each other.

In this experiment, the magnetic microspheres with 20 μm in diameter and polystyrene microspheres with 50 μm in diameter were inserted into the microfluidic chip full of deionized water. The signal source was a $10V_{pp}$ bias voltage with an AC frequency of 100 kHz. Subsequently, the OET platform was employed to transport 20 μm positive dielectric magnetic microspheres to interact with 50 μm negative-dielectric polystyrene microspheres, as shown in Fig. 5b. Followed by the trapping with the light spot, the magnetic microspheres adhered to the polystyrene microspheres and could be joined into assemblies of multiple microsphere pairs. Magnetic microspheres were then trapped by the light spot and employed to transport the combined adhered particles at the velocity of 21.56 μm s^{-1}, as shown in Movie S5.† The manipulated force can reach 4.06 pN. When the one polystyrene microsphere transports the two magnetic microspheres to the target position, the velocity is 22.27 μm s^{-1}. Finally, the negative-dielectric polystyrene microspheres were released from the positive-dielectric magnetic microspheres after withdrawing the input voltage signal. As shown in Fig. 5c, the speed of moving the non-adhered particles is not much different from the speed of moving the adhered particles. It indicates that adhered particles can be transported more efficiently under the same conditions. In addition, one particle can interact with different particles, as shown in Fig. 5e. By control the interaction, particles do not only form a chain. We could assemble some special structures with different particles, such as microrobots. The maximum number of the interaction of particles is 8. This relation is also presented in Fig. 5d, in which the velocity of transportation for a given input condition and illumination power would not be significantly affected by the number of adhering particles. Under this condition, the number of adhering particles that can be transported can be increased by adjusting the voltage and power, which implicates that one particle can interact with multiple particles at the same time.

2.4 Interaction between microorganism and particle

Euglena gracilis, a versatile phototrophic protist, characterized by the tolerance to many extremely external stresses, like acidic

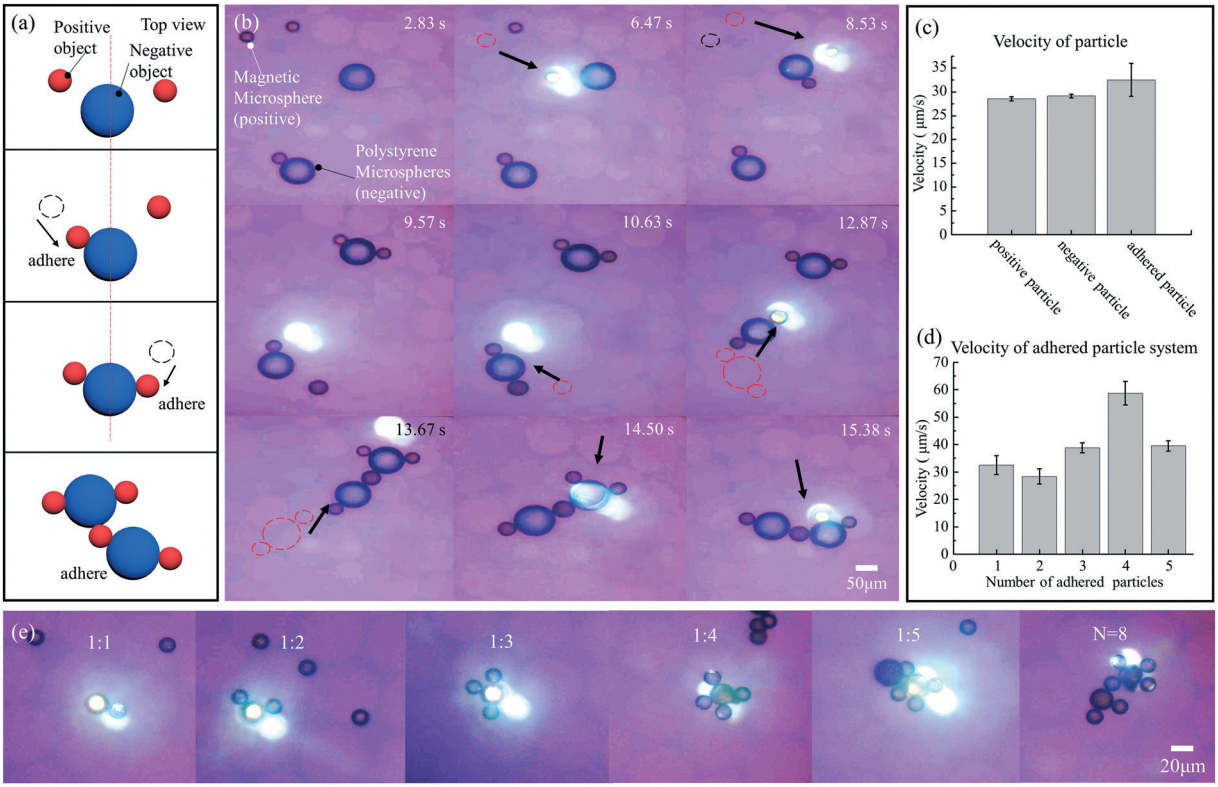

Fig. 5 Controllable positive-dielectric micro-object interacts with multiple negative-dielectric microparticles *via* OET. (a) Schematic of the interaction between polystyrene microbeads and magnetic particles. (b) Polystyrene microbeads interact with magnetic particles and transportation *via* polystyrene microbeads. (c) Transport velocities of different types of particles. (d) The relationship between the number of interacted particles and transport velocity. (e) One particle interacts with a different number of particles.

growth conditions,[45] has been employed for application-driven.[46] Similarly, spirulina has been extensively employed for some purposes, such as drug delivery,[47] and the preparation of special materials.[48] To assess the applicability of the OET platform in achieving the interaction between microorganisms with complex shapes and particles, swimming *E. gracilis* and microspirulina were selected as agents to interact with particles and achieve the transport and release of particles at the target position. Due to the microorganism is swimming and the shape is more complex than the microbeads, to precisely manipulate the interaction between microorganisms and microparticles, the direction of alignment of *E. gracilis* along the vertical plane was adjusted *via* changing the input frequency, as shown in Fig. 6a. In this figure, θ represents the angle of the microorganism relative to the bottom substrate. In the OET chip environment, *E. gracilis* will principally be affected by torques from dielectrophoresis, viscosity, and gravitational forces. Based on the shape of *E. gracilis*, the angle in the vertical plane of the organism relative to the bottom substrate can be calculated as follows:

$$\cos\theta = \frac{d}{L} \tag{1}$$

where L represents the length of *E. gracilis* and d represents its projected length along the bottom substrate, which can be measured with a microscope ruler.

The relationship between the applied frequency and the orientation of the *E. gracilis* can be obtained by altering the frequency over the range of 1 kHz to 60 MHz. As shown in Fig. 6a, at frequencies of 100 kHz, 10 MHz, and 60 MHz in deionized water, the angle in the vertical plane of the organism relative to the bottom substrate is 90°, 50°, and 0°, respectively. These results indicate that, with other conditions remain constant, the dielectrophoresis torque would initially increase with freqency[49] and then, after reaching a threshold, decrease with frequency. It means that the working frequency range is 100 kHz to 1 MHz for this microorganism. The relationship between manipulated DEP force and input frequency is shown in Fig. 6b. The results show that *E. gracilis* could be transported at a working frequency range. When the input frequency is low, the generated DEP force is not enough to manipulate *E. gracilis* due to the resistance from its swimming.

The *E. gracilis* combined with polystyrene microbeads were injected into the chip full of deionized water for interaction. In this experiment, the frequency was set as 100 kHz. Prior to the application of the electric field, *E. gracilis* was able to swim at a velocity of 63.80 μm s^{-1}. With the application of AC electric field, *E. gracilis* rotated from a horizontal orientation to vertical orientation, which is in line with the direction of the electric field. Fig. 6c presents a comparison of the manipulated velocities of *E. gracilis* and polystyrene

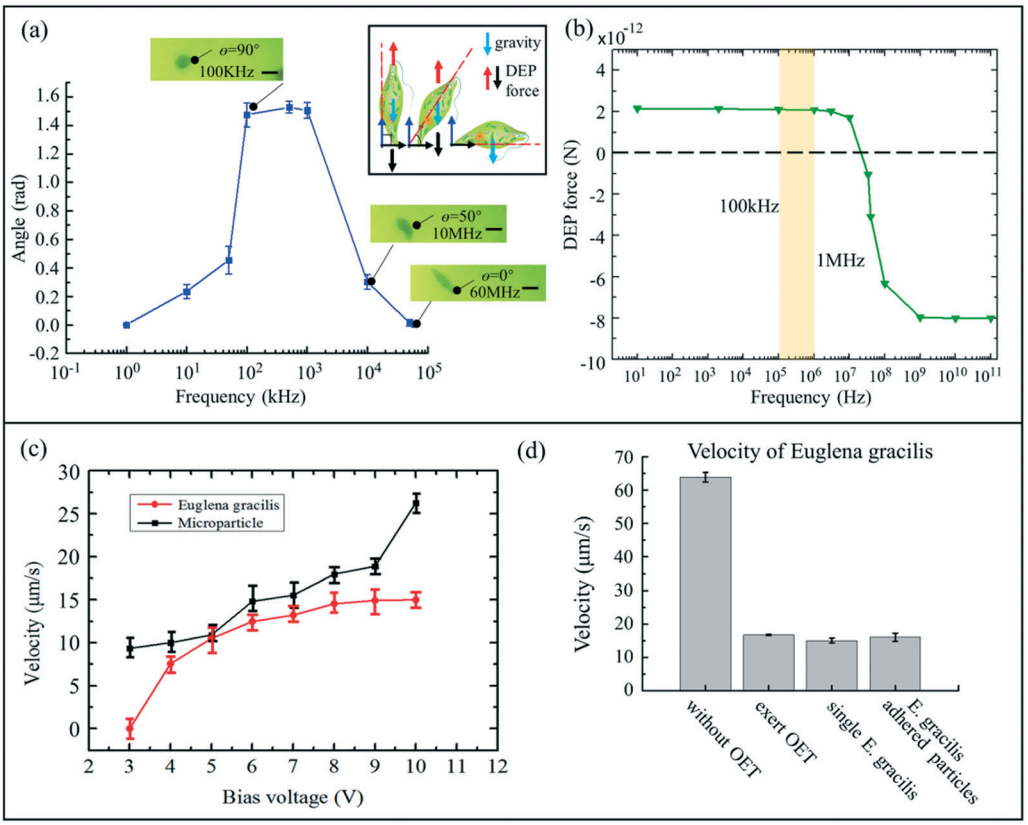

Fig. 6 Changes in electrophoresis force on *E. gracilis* with input frequency and velocity of manipulation. (a) The direction of *E. gracilis* in deionized water at different frequencies. (b) The relationship between DEP force and input frequency. (c) The OET-induced velocity of manipulation. (d) Movement velocity of microorganisms under different conditions.

microspheres under different voltages. In both cases, the velocities increase sharply with the voltage. Due to the active swimming of *E. gracilis*, their manipulated velocities are less than those of microparticles.

A schematic of the interaction between polystyrene microbeads and *E. gracilis* is shown in Fig. 7a. The input voltage is $10V_{pp}$. *E. gracilis* was able to swim at a velocity of 16.73 μm s^{-1} under the electric field. Then, the trapping within the light spot left them stationary and able to engage only in vibration around a central point; during the transport process, the microorganisms moved at approximately 15.03 μm s^{-1}. The manipulated force of *E. gracilis* is 6.18 pN. These microorganisms were then trapped by the light spot to adhere with 15 μm polystyrene microbeads, and transported through the chip at a velocity of 16.06 μm s^{-1}, as shown in Fig. 6d. The overall interaction process is shown in Fig. 7b. Movie S6† presents an example of swimming *E. gracilis* that is interacted with 15 μm polystyrene microbeads and is used as agents to transport polystyrene microbeads. Compare with the conventional dipole moment in the sphere particle, the rod-shaped *E. gracilis* could generate a changing dipole moment when it rotated in the medium. After these experiments, *E. gracilis* did not display adverse reactions in terms of, for example, membrane damage.

Then, the complex shape of microspirulina was also used to interact with microbeads, as shown in Fig. 7c. After the injection of microspirulina combined with polystyrene microbeads into the microfluidic chip, an input signal with the voltage and frequency of $10V_{pp}$ and 100 kHz, respectively, was applied. The microorganisms were manipulated by the OET light pattern to realize the interaction with the polystyrene microbeads and the transport of microbeads along the device plane, as shown in Fig. 7d. Movie S7† presents the transport of microspirulina, in which the movement velocity of the spirulina-particle assemblies is approximately 14.79 μm s^{-1}. It is subjected to a DEP force of 3.12 pN. Furthermore, the spirulina is also able to transport two or more particles at once on account of its special spiral structure, although the movement velocity of the spirulina would decrease with the increase in the number of transported particles. For the polarization in the helical structure, it could be analyzed by the infinitesimal method or vector sum over all the dipoles. The results indicate that microorganisms (such as swimming *E. gracilis* and microspirulina) can be employed to transport objects to a target position by applying complementary forces on particles with opposite dielectric properties *via* OET system.

3. Experimental

3.1 Fabrication of a-Si film and microfluidic chip

Commonly, a-Si:H films are fabricated on indium tin oxide (ITO) glass *via* plasma-enhanced chemical vapor deposition

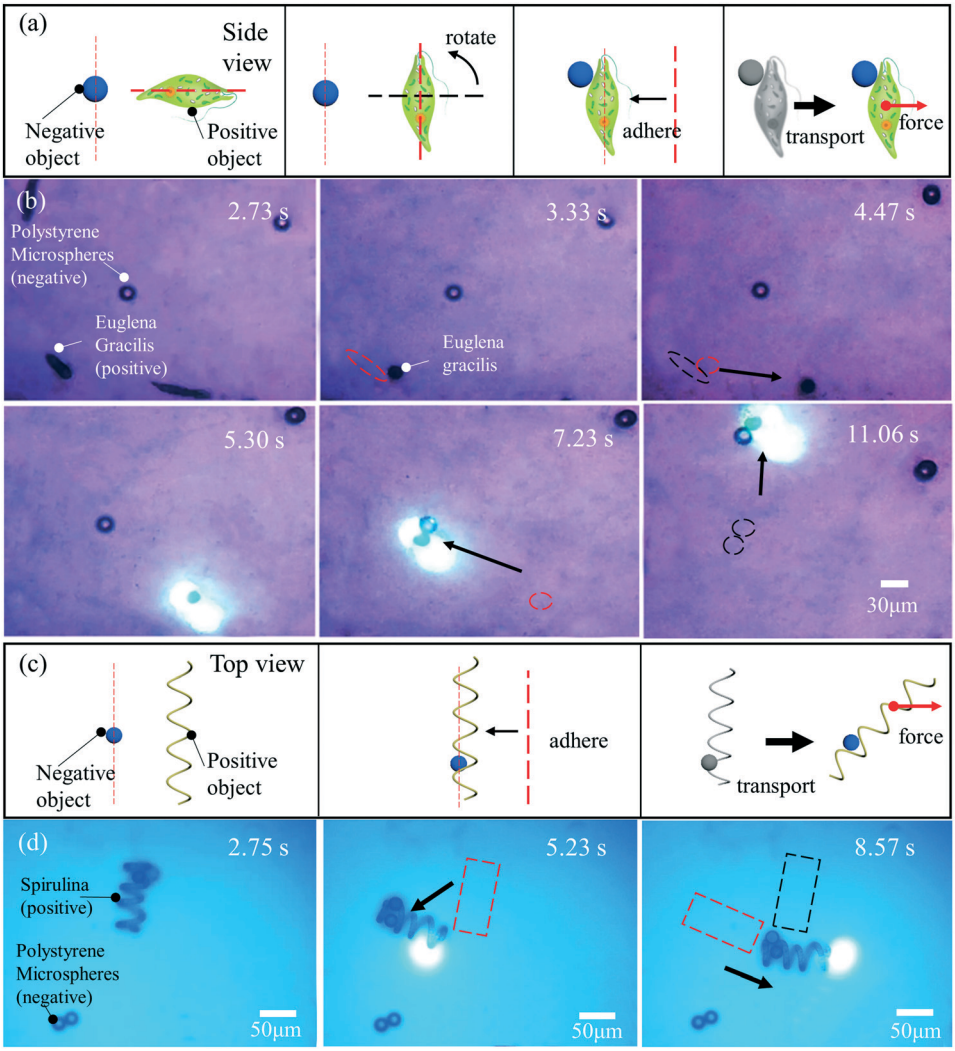

Fig. 7 Microorganisms with positive dielectric properties interact with micro-objects *via* OET. (a) Schematic of the interaction between polystyrene microbeads and *E. gracilis*. (b) The interaction between polystyrene microbeads and *E. gracilis* and the transportation of polystyrene microbeads with *E. gracilis*. Circles and black arrows represent previous positions on the plane and direction of movement, respectively. (c) Schematic of the interaction between polystyrene microbeads and micro-spirulina. (d) The transportation of polystyrene microbeads with spirulina. Rectangles and black arrows represent the previous position on the plane and the direction of movement, respectively.

(PECVD).[14,50,51] In this study, the traditional a-Si:H film was adopted to build the microfluidic chip in the OET, as shown in Fig. S12a.† The chip consists of the top electrode (ITO), the space of medium (the thickness is 150 μm), and the bottom electrode, which is ITO glass coated with a-Si:H film (the thickness is 1 μm). In addition, in order to simplify the traditional fabricated process and save costs, the a-Si film was also fabricated *via* sputtering[52–55] for its application in a microfluidic chip. The ITO glass was ultrasonically cleaned with absolute ethanol for 10 min and with deionized water for a further 10 min, and then it was dried and treated with a plasma cleaner for 20 s to enhance the adhesion of the a-Si film to the ITO. The ITO was placed at the central substrate of a sputter instrument. At a sputter instrument vacuum of 10^{-5} Pa, Ar gas flux of 0.8 Pa s^{-1}, and substrate temperature of 25 °C, AC magnetron sputtering was applied at 150 W for 2 h. After finished sputtering, a a-Si film was placed in a muffle furnace and annealed at 300 °C for 1 h under nitrogen protection. Finally, a stable 1.5 μm-thick a-Si film was successfully fabricated.

3.2 OET system setup and wireless control

The structure of the OET system was designed in this study, as shown in Fig. S12b.† This system is composed of three parts. Firstly, the image projected part is the blue path. A digital micromirror device (DMD) projector (BenQ E580, China) is adopted to generate a light pattern. The light pattern propagates through two lenses (L1 and L2), a reflecting mirror (M), and a condenser lens (L3). It would project an ITO electrode (NOZO Co., China) including a photoconductive layer. Thus, the light pattern can be applied for real-time manipulation. Secondly, the illuminated part is the yellow path. The light from an LED would be collected as

a straight beam through a focusing lens (L6) and it propagates through PBS, and an objective lens (L4), illuminating the chip. Thirdly, the experimental observation part is the black path. The experimental image propagates through the objective lens (L4) and lens (L5). It would be projected in a charge-coupled device (CCD) camera (GS3-U3-23S6C-C; Canada) for recording. In addition, a function generator was adopted to generate AC voltages. A computer was used to produce a pattern on the DMD-based projector.

To realize convenient control of the OET, the wireless-control platform was established, with the scheme shown in Fig. S13a.† The platform is composed of a Cloud server, multi-platform interactive terminals, and an executive terminal including the OET equipment. The Cloud server could bear massive time-consuming computational loads, such as image processing, projected graphic generation, and data format conversion. The interactive terminals include cross-platform graphic user interfaces (GUIs), which are equipped by an iPad and PC to enable efficient interaction between operators and the OET system. The executive terminal is a PC connected to the microscope and projector, which is responsible for sending control signals to the experimental equipment and receiving the feedback information. The three modules were deployed under a wireless local area network and engaged in safe communication based on the WebSocket protocol. The applied wireless-data transmission principles are shown in Fig. S13b.† With the adoption of the WebSocket protocol, full-duplex communication channels could be achieved under a single TCP connection and the use of HTTP protocol could be avoided. Meanwhile, a standard GUI program was developed for the OET system, in which the tasks of real-time CCD camera monitoring, design, and control of projected graphics, post-processing of acquired microscope images, and recognition result display can be integrated.

3.3 Preparation of microorganism samples

E. gracilis (50 μm to 100 μm in length) was cultured at room temperature. 10 μl of *E. gracilis* medium and 10 μl of the 15 μm-diameter polystyrene microbeads medium were mixed *in vitro* and poured into 1 ml deionized water. 10 μl of the mixed liquid was inserted into the chip with a pipette. Microspirulina is a spiral-shaped aquatic plant with a length from 52 μm to 360 μm. The helical thread diameter of microspirulina is about 5–8 μm. 10 μl of the microspirulina medium was mixed *in vitro* with 15 μm-diameter polystyrene microbeads in a 10 μl solution and poured into 1 ml of deionized water, from which 10 μl droplets of the mixed liquid were extracted and placed into the chip of OET with a pipette.

4. Conclusions

In this paper, an exploration was performed on the interaction between different micro-objects in a simple OET platform. At first, the interaction between particles was simulated by the ALE method (including positive DEP and negative DEP effect). An analysis was performed on the key parameters of interaction, which provided instruction for the experiment. Subsequently, an iPad-hosted wireless-control interface was designed for convenient control. The system can be established *via* a simple process and used to manipulate multiple particles simultaneously with a very low power intensity in a fabricated microfluidic chip. During the interaction experiments, one particle can interact with 5 particles simultaneously, which indicates that the interaction can be applied to improve high-throughput transportation capacities and assemble some special microstructures with particles. Then, swimming *E. gracilis* and spirulina were selected to interact with particles with opposite dielectric properties. These microorganisms were also used as an agent for the transport of polystyrene microbeads to a target position and the subsequent release after withdrawing the electric field. It shows that the micro-objects with complex dimensionalities and topologies, including spherical polystyrene microspheres, rod-shaped *E. gracilis*, and spiral-shaped microspirulina, can be employed to interact in the OET system. Due to the low power levels, those microorganisms were free from damages during those experiments. It is expectable that the interaction between particles in the simple OET platform could be employed in medical applications involving the detection of cancers or viruses, drug release, and a wide range of similar tasks.

Author contributions

There S. L. and C. G. contributed equally to this work. There S. L. and Y. D. designed and built the OET system, performed the experiments (with assistance from L. F.). S. L., C. G., and C. Z. designed and ran the simulations, evaluated the data. S. L., C. G., and X. B. prepared the figures (with assistance from H. C. and L. F.). S. Z. and A. R. W. designed and fabricated the a-Si:H film. H. C. and L. F. coordinated and supervised the work. S. L., C. G., and L. F. wrote and edited the manuscript. All authors provided feedback on the manuscript.

Conflicts of interest

There are no conflicts to declare.

Acknowledgements

This work was supported by the National Key R&D Program of China (Grant No. 2019YFB1309700) and the Beijing Nova Program of Science and Technology (Grand No. Z191100001119003).

Notes and references

1 S. R. Khetani and S. N. Bhatia, *Nat. Biotechnol.*, 2008, **26**, 120–126.
2 A. M. Skelley, O. Kirak, H. Suh, R. Jaenisch and J. Voldman, *Nat. Methods*, 2009, **6**, 147–152.

3 S. Mohanty, *Lab Chip*, 2012, **12**(19), 3624–3636.
4 F. Lin, D. Pei and F. Arai, *Int. J. Rob. Res.*, 2016, **35**, 1445–1458.
5 F. Lin, S. Liang, X. Zhou, J. Yang, Y. Jiang, D. Zhang and A. Fumihito, *Appl. Phys. Lett.*, 2017, **111**, 203701–203705.
6 Y. Dai, S. Liang, Y. Chen, Y. Feng, D. Chen, B. Song, X. Bai, D. Zhang, L. Feng and F. Arai, *Advanced Intelligent Systems*, 2020, **2**, 1900148–1900158.
7 L. Feng, B. Song, D. Zhang, Y. Jiang and F. Arai, *Micromachines*, 2018, **9**, 596–607.
8 C.-T. Ho, R.-Z. Lin, W.-Y. Chang, H.-Y. Chang and C.-H. Liu, *Lab Chip*, 2006, **6**, 724–734.
9 P. Gascoyne, C. Mahidol, M. Ruchirawat, J. Satayavivad, P. Watcharasit and F. F. Becker, *Lab Chip*, 2002, **2**, 70–75.
10 A. Ashkin, J. M. Dziedzic and T. Yamane, *Nature*, 1987, **330**(6150), 769–771.
11 D. G. Grier, *Nature*, 2003, **424**, 810–816.
12 M. L. Juan, M. Righini and R. Quidant, *Nat. Photonics*, 2011, **5**, 349–356.
13 K. Svoboda and S. M. Block, *Annu. Rev. Biophys. Biomol. Struct.*, 1994, **23**, 247–285.
14 P. Y. Chiou, A. T. Ohta and M. C. Wu, *Nature*, 2005, **436**, 370–372.
15 S. Zhang, N. Shakiba, Y. Chen, Y. Zhang, P. Tian, J. Singh, M. D. Chamberlain, M. Satkauskas, A. G. Flood and N. P. Kherani, *Small*, 2018, **14**, 1803342–1803349.
16 A. Yunus, Y. Berk, B. Onur, F. D. Ahmet and S. Metin, *Nat. Mater.*, 2019, **18**, 1244–1251.
17 H. Hwang and J. K. Park, *Lab Chip*, 2011, **11**, 33–47.
18 L. Y. Ke, Z. K. Kuo, Y. S. Chen, T. Y. Yeh, M. Dong, H. W. Tseng and C. H. Liu, *Lab Chip*, 2017, **18**, 106–114.
19 H. Hwang, Y. J. Choi, W. Choi, S. H. Kim, J. Jin and J. K. Park, *Electrophoresis*, 2008, **29**, 1203–1212.
20 A. Jamshidi, P. J. Pauzauskie, P. J. Schuck, A. T. Ohta, P. Y. Chiou, J. Chou, P. Yang and M. C. Wu, *Nat. Photonics*, 2008, **2**, 86–89.
21 S. M. Yang, T. M. Yu, H. P. Huang, M. Y. Ku and C. H. Liu, *Opt. Lett.*, 2010, **35**, 1959–1961.
22 Z. Shuailong, Y. S. Erica, S. Jastaranpreet, C. Yujie and R. W. Aaron, *Proc. Natl. Acad. Sci. U. S. A.*, 2019, **116**, 14823–14828.
23 C. Witte, C. Kremer, M. Chanasakulniyom, J. Reboud, R. Wilson, J. M. Cooper and S. L. Neale, *Small*, 2014, **10**, 3026–3031.
24 W. Yang, H. Yu, G. Li, Y. Wang and L. Liu, *Small*, 2017, **13**, 1602769–1602776.
25 M. B. Lim, R. G. Felsted, X. Zhou, B. E. Smith and P. J. Pauzauskie, *Appl. Phys. Lett.*, 2018, **113**, 031106–031112.
26 M. Li, N. Liu, P. Li, J. Shi, G. Li, N. Xi, Y. Wang and L. Liu, *ACS Appl. Mater. Interfaces*, 2017, **9**(9), 8361–8370.
27 S. Glaesener, M. Esseling and C. Denz, *Opt. Lett.*, 2012, **37**, 3744–3746.
28 S. L. Neale, N. Mody, C. Selman and J. M. Cooper, *Proc. SPIE*, 2012, **8458**, 27–35.
29 T. R. M. A. Mishra, T. M. Walter, A. Wei, S. J. Williams and S. T. Wereley, *Lab Chip*, 2016, **16**, 1039–1046.
30 T. Jones, *Electromechanics of particles*, Cambridge University Press, 1995.
31 H. Hwang, J. J. Kim and J. K. Park, *J. Phys. Chem. B*, 2008, **112**, 9903–9908.
32 Y. Chen, A. F. Sprecher and H. Conrad, *J. Appl. Phys.*, 1992, **70**, 6796–6803.
33 S.-Y. Kang and A. S. Sangani, *J. Colloid Interface Sci.*, 1994, **165**(1), 195–211.
34 T. S. Simonova, V. N. Shilov and O. A. Shramko, *Colloid J.*, 2001, **63**, 108–115.
35 M. Finessi, I. Szilagyi and P. Maroni, *J. Colloid Interface Sci.*, 2014, **417**, 346–355.
36 Y. Ai and S. Qian, *J. Colloid Interface Sci.*, 2010, **346**, 448–454.
37 H. A. Pohl, *Dielectrophoresis: the behavior of neutral matter in nonuniform electric fields*, Cambridge University Press, 1978.
38 T. B. Jones, *J. Appl. Phys.*, 1986, **60**, 2226–2230.
39 T. B. Jones, *Electromechanics of particles*, Cambridge University Press, 1995, ISBN: 0521431964 hardback.
40 R. Tao, Q. Jiang and H. K. Sim, *Phys. Rev. E: Stat. Phys., Plasmas, Fluids, Relat. Interdiscip. Top.*, 1995, **52**, 2727.
41 H. H. Hu, N. A. Patankar and M. Y. Zhu, *J. Comput. Phys.*, 2001, **169**, 427–462.
42 T. Z. Jubery, S. K. Srivastava and P. Dutta, *Electrophoresis*, 2014, **35**, 691–713.
43 S. Liang, Y. Cao, Y. Dai, F. Wang, X. Bai, B. Song, C. Zhang, C. Gan, F. Arai and L. Feng, *Micromachines*, 2021, **12**, 271.
44 L. Liu, C. Xie, B. Chen and W. U. Jiankang, *J. Appl. Math. Mech.*, 2015, **36**, 1499–1512.
45 T. Ishikawa, N. Tajima, H. Nishikawa, Y. Gao, M. Rapolu, H. Shibata, Y. Sawa and S. Shigeoka, *Biochem. J.*, 2010, **426**, 125–134.
46 K. Bishal, K. Liisa, S. Anwar, S. Angela and N. Helena, *Algal Res.*, 2019, **37**, 178–185.
47 X. Wang, J. Cai, L. Sun, S. Zhang, D. Gong and X. Li, *et al.*, *ACS Appl. Mater. Interfaces*, 2019, **11**, 4745–4756.
48 X. Li, J. Cai, Y. Shi, Y. Yue and D. Zhang, *ACS Appl. Mater. Interfaces*, 2017, **9**, 1593–1601.
49 H. Morgan and N. G. Green, *AC electrokinetics: colloids and nanoparticles*, Research Studies Press, 2003, ISBN: 0863802559.
50 X. Q. Zhang, W. J. Zhang, M. L. Wu, S. L. Jia, H. Liu and L. I. Guo-Hua, *Journal of Functional Materials*, 2007, **10**, 1741–1744.
51 H. J. Kim and H. J. Lee, *J. Appl. Phys.*, 2018, **123**, 113301–113316.
52 P. M. Martin and W. T. Pawlewicz, *Sol. Energy Mater.*, 1980, **2**, 143–157.
53 N. Serin, *J. Phys. D: Appl. Phys.*, 1984, **17**, 1485–1492.
54 S. Klein, M. Rohde, S. Buschbaum and D. Severin, *Sol. Energy Mater. Sol. Cells*, 2012, **98**, 363–369.
55 Y. H. Kim, W. K. Kim, J. I. Han and D. G. Moon, *J. Soc. Inf. Disp.*, 2012, **15**, 1105–1108.